Title:

A study on the cell structure and the performances of wall-flow diesel particulate filter

Authors:

K. Tsuneyoshi [a,b] and K. Yamamoto* [b]

Affiliation:

[a] Environmental Materials R&D Center, TYK Corporation
3-1 Ohbata-cho, Tajimi-shi, Gifu 507-8607, Japan
[b] Department of Mechanical Science and Engineering, Nagoya University
Furo-cho, Chikusa-ku, Nagoya-shi, Aichi 464-8603, Japan

Type of article:

Full length article

Address of the corresponding author

Department of Mechanical Science and Engineering, Nagoya University
Furo-cho, Chikusa-ku, Nagoya-shi, Aichi 464-8603, Japan
telephone number: +81-52-789-4471
fax number: +81-52-789-4471
e-mail: kazuhiro@mech.nagoya-u.ac.jp

Abstract

As for the recent PM regulations, a diesel particulate filter (DPF) has been one of the important aftertreatment technologies. Although the square cell structure of DPF is a generally worldwide standard, several cell designs have been proposed to reduce the pressure loss due to the soot loading as well as the ash deposition in DPF. In this study, we focused on the cell geometry using a hexagonal cell DPF and a conventional square cell DPF. In the engine test bench under nearly real conditions, these DPF performances were evaluated. Results show that, in comparison with square cell DPF, the particle number concentration of the hexagonal cell DPF decreases more rapidly, and the filtration efficiency is higher. In addition, in DPF regeneration test, independent of the inlet temperature, the regeneration rate of the hexagonal cell DPF is higher. Between two DPFs, the aperture ratio of inlet/outlet cells is different. Thus, the superior DPF performance of the hexagonal cell DPF could be explained by the difference of exhaust gas flow and soot deposition region.

Key words:

Diesel particulate filter; Diesel engines; Emission control; Filtration efficiency; Pressure drop; Regeneration

1. Introduction

Diesel engines have low fuel consumption and enough torque compared with equivalent gasoline engines. Diesel engines emitted less CO_2 which is known well as the greenhouse gas, and a percentage of new diesel passenger car registrations is increasing in EU year by year [1]. However, NOx and the soot (particulate matter, PM) emitted by the diesel engines cause problems such as air pollutions and asthma sickness [2]. Since the automobile regulations have been stricter for considering environments and human health [3], new technologies for the diesel emission have been proposed. For example, improvements on the fuel injection for the combustion process [4,5], exhaust gas recirculation (EGR) [6,7], and the engine control [8,9] are effective for the NOx and PM reduction. In addition, some kinds of fuel additive have been used for the diesel smoke reduction [10-12]. The PM can be reduced by using water containing ethanol-biodiesel [13]. Moreover, the inlet manifold water injection has been also investigated for the NOx and PM reduction of an automotive direct injection diesel engine [14].

As for the current regulations, the European Union restricts PM emissions to 5

mg/km for passenger diesel cars in the EURO 5 and 6 regulations. Furthermore, the basis of PM emission regulations is being changed from mass to number concentration [15]. A diesel particulate filter (DPF) is one of the most important technologies for the above strict PM regulations [16]. Figure 1 shows the image of a wall-flow DPF made of the structured porous ceramic. It has many flow path channels called “cells”, and the exhaust gas is flown into cells. PM in exhaust gas is trapped on the surface of the wall when the exhaust gas is passed through the porous wall.

The DPF needs low pressure loss for the lower fuel consumption. Since the pressure loss increases by the formation of a thick soot cake as the soot is accumulated, the DPF needs to be periodically regenerated by burning off the accumulated soot. Therefore, DPF is mainly demanded three performances - filtration, pressure drop, and regeneration. Torregrosa et al. have proposed the model about the relationship of these DPF performances [17]. In particular, Payri et al. have evaluated the pore structure properties – permeability, porosity, and pore size, on experimental - theoretical methodology, because the pressure drop and the filtration process are strongly depending on these properties [18]. Dilip et al. have developed a mesh-type particulate

filter for the regeneration required lower input power [19]. However, the filtration efficiency of the mesh-type particulate filter has not reached to the level of the strict regulations.

On the other hand, a lot of regeneration cycles cause the ash, which is the remaining of soot burning [20]. The ash is formed all along the filter walls of the inflow channels; and it induces the increase of the pressure loss [21]. The pressure loss also increases by the ash accumulation, and it is considered that the regeneration cycle is shortened by the ash accumulation [22].

Although the square cell DPF is a generally worldwide standard, several cell designs have been proposed to prevent the pressure loss from increasing by soot loading and to reduce the effect of the ash deposition. Ogyu et al. have reported that the increase of the pressure loss with the soot loading and the ash deposition can be controlled to be lower by changing the aperture ratio of inlet cells. In particular, the octagon-square cell DPF has superior performances on the pressure loss during the soot loading and the ash capacity, compared with the conventional square cell DPF [22,23]. At present, such DPFs that have specially shaped cells have been realized with advance of manufacturing

technologies.

In our previous studies, we have examined an initial PM filtration efficiency, and have confirmed that the soot leakage is reduced due to the soot layer formation on the surface of the filter wall during the initial usage of the clean DPF. Additionally, the washcoat (W/C) samples for the catalyzed DPF, we have found that there is a proper range of the W/C amounts in terms of the W/C amounts and the pressure loss [24]. Amirnordin et al. have investigated a honeycomb monolith with hexagonal cell, and have reported that its pressure loss is relatively low [25]. However, they have focused on catalytic converters. It is not clear that the effect of the cell structure on the DPF performance. Therefore, in this study, we focused on the cell geometry by using a hexagonal cell DPF and a conventional square cell DPF to evaluate the DPF performances. The experimental study was carried out. As for the conditions of the engine test, we set the medium speed with high torque (1400 rpm 190 Nm) for the soot loading, and the high speed (3000 rpm) for the DPF regeneration [26].

2. Experimental methods

2.1.DPF

Two silicon-carbide (SiC) DPFs were prepared in this study. The specifications of two DPF samples are shown in Table 1, and their appearances and cell designs are shown in Fig. 2. Sample A has hexagonal cells, and sample B has conventional square cells. Two samples are non-catalytic filters. For each sample, size is Φ144 mm × L153 mm, cell density is 300 cpsi, and wall thickness is 0.25 mm. The pore structure characteristics were measured by mercury porosimetry (MICROMERITICS Co. AutoPore 9500), and showed that porosity and average pore diameter were almost the same.

2.2. Measurement of PM filtration efficiency

The filtration efficiency of the DPF was evaluated with a QD32 diesel engine (NISSAN). Table 2 shows the engine specifications. The engine was connected to an eddy current dynamometer (Tokyo Plant Co. ED-150) on the test-bench for the test condition at 1400 rpm and 190 Nm load. A schematic of the experimental setup is shown in Fig. 3. A diesel oxidation catalyst (DOC; ACR Co. EXCAT C15) was set

upstream of the DPF. To measure the particle number concentration and the particle size distribution in the exhaust gas, an engine exhaust particle sizer (TSI Co. EEPS 3090) was used in conjunction with a flow path selection system to obtain the data downstream of the DPF [27,28]. Generally, the EEPS can measure the particle number concentration in the range from 10^3 to 10^7 particles/cm^3. The sampling particles are electrical charged, and are distributed in the range from 5.6 to 560 nm based on differential electrical mobility classification [29]. The data from EEPS or pressure sensor was recorded by 10 data per second. The sampling gas was diluted by 120 times using 350 °C air in a dilution machine (TSI Co. ASET). For reference, a flange with orifices was used without DPF downstream of the EEPS conjunction point for the equivalent backpressure of the DPF.

2.3. Measurement of backpressure and amounts of soot loading

The pressure loss during soot loading was measured as the backpressure by a pressure sensor (KEYENCE Co. AP-32A) in front of the DPF. The measurement range of the pressure sensor is from 0 to 100 kPa, with the resolution of 0.1 kPa. We also

measured the initial backpressure under the cold flow condition with 4, 6, 9, 9.5 Nm^3/min. The amount of soot loading was calculated based on the difference of the DPF weight every 15 minutes driving. In experiments, the DPF with canning was got off from the exhaust pipe, and the weight was measured by an electronic balance. Its resolution was 0.1 g.

2.4. DPF regeneration test

Each sample was loaded with 8 g/L soot for the test condition at 1400 rpm and 190 Nm load. Temperature and oxygen conditions were kept constant for 30 minutes by using the exhaust gas to burn off the soot for regeneration. Such a controlled DPF regeneration is often called “active regeneration” [26]. The amount of burned soot and the regeneration rate were calculated based on the DPF weight after the regeneration test. Three thermocouples were inserted at the front area, the middle area, and the rear area of the DPF, as shown in Fig. 4. A set of K-type thermocouples was used. We controlled the DPF inlet temperature located at ch3 in this figure. Three test conditions

were selected at different inlet temperatures of 510, 550, and 590 °C at the engine speed of 3000 rpm. We also measured the oxygen concentrations using an oxygen sensor (COSMOS Co. XP-3180E). These test conditions are shown in Table 3.

3. Results

3.1. Time variations of PM filtration efficiency

Figure 5 shows the number-based filtration efficiency upon the initial usage. The time was counted when the particle number concentration downstream of the DPF reached the maximum after the engine accelerator was released. Filtration efficiency was calculated by:

$$\text{Filtration efficiency} = \left(1 - \frac{N_1}{N_0}\right) \times 100 \qquad (1)$$

where N_0 is the total particle number concentration without the DPF, which is the time-averaged number concentration in stable engine condition, and N_1 is the total particle number concentration downstream of each DPF. The filtration efficiency based

on the particle concentration was checked several times, and the error was less than 3 percent. Although the filtration efficiencies for both samples are initially about 70 %, more particles are trapped by sample A with higher filtration efficiency as the time is passed. After 180 seconds, the filtration efficiency is approximately 100 %, which is caused by the surface filtration due to the soot layer formation. Therefore, the better filtration efficiency of the hexagonal cell DPF could be explained by the process of soot layer formation, which will be discussed later.

In our previous study [24], we have introduced new parameters: T90 and T99; where T90 (T99) is the time to reach more than 90 % (99 %) filtration efficiency. The smaller these parameters, the less PM leakage are achieved with higher filtration efficiency. Figure 6 shows T90 and T99 of samples A and B. In comparison with sample B, T90 and T99 of sample A are much smaller. Resultantly, the filtration efficiency of the hexagonal cell DPF is higher. As seen in Table 1, since these two DPFs have approximately the same properties of the porosity and the pore size, the cell geometry surely affects the PM filtration efficiency.

3.2. Comparison of backpressure

Figure 7 shows the relationship between the initial backpressure and the air flow rate of each sample. As the air flow rate increases, the initial backpressure monotonically increases. This tendency corresponds with the results conducted by the numerical simulation and experiments [30]. In addition, it is seen that the initial backpressure of sample A is always higher than that of sample B. Figure 8 shows the backpressure during soot loading of each sample. Although the initial backpressure of sample A is higher than that of sample B, the backpressure during the soot loading of two samples are almost equal at approximately 2 g/L soot loading. When the amount of soot loading is larger than 2 g/L, the backpressure of sample A is lower than that of sample B.

Figure 9 shows the relationship between the soot loading time and the amount of soot loading for each sample. For both cases, the amount of soot loading increased almost linearly. Interestingly, the amount of soot loading did not depend on the cell geometry.

3.3. Regeneration rate

Next, we examined the amount of the burned soot in the DPF regeneration process. Figure 10 shows the time variation of the temperatures inside of the DPF (ch1: inlet side, ch2: center, ch3: outlet side) and the backpressure during the regeneration test. The inlet temperature was maintained at 590 °C (test condition 3). For comparison, the results of both samples are shown. It is found that the backpressure gradually decreases once the temperature inside the DPF reaches 590 °C. That is, the deposited soot inside the DPF is burned off, and the DPF is regenerated. For both cases, the temperatures inside the DPF are almost uniform during regeneration. Also, the decrease of the backpressure is almost constant. Then, the DPF is regenerated at the same combustion rate.

Figure 11 shows the comparison of the regeneration rate of two samples at different inlet temperature. The regeneration rate was calculated by:

$$\text{Regeneration rate} = \left(\frac{M_1}{M_0}\right) \times 100 \qquad (2)$$

where M_0 is the total amount of accumulated soot before regeneration, and M_1 is the amount of burned soot during regeneration. As the inlet temperature of the DPF is higher, the regeneration rate also increases.

Song et al. have reported a relationship between the DPF inlet temperature and the rate of pressure drop during the regeneration; and the better regeneration is achieved at the higher inlet temperature [31]. Lee et al. have reported that the soot combustion is affected by the oxidation concentration of the exhaust gas [32]. In our previous study, we have confirmed that the soot oxidation rate varies with oxygen concentration [33]. In addition, the soot oxidation is largely intensified at higher temperature [34]. Table 3 shows that more soot is burned off at higher inlet temperature although the oxygen concentration is lower at higher inlet temperature. Interestingly, independent of the inlet temperature, the regeneration rate of sample A with the hexagonal cells is higher than that of sample B with the conventional square cells. Therefore, the effect of the cell geometry on the DPF regeneration rate is confirmed.

4. Discussions

Table 4 shows the comparison of the test results, where the circle symbol in this table means that which sample is more superior on each specification. In comparison with sample B, sample A had the higher initial PM filtration efficiency, the lower backpressure during soot loading, and the higher regeneration rate. Here, we discuss the difference of the filter structure and characteristics.

As for the initial PM filtration usage, it is considered that the effective filtration area of the gas flow of sample A is smaller than that of sample B. In the case of sample B, the gas flows from the inlet cell to the surrounding outlet cells in four directions. On the other hand, in the case of sample A, the gas hardly flows the filter wall between the inlet cell and the inlet cell, but flows in three directions from the inlet cell to the outlet cells (flow 1 shown in Fig. 12 (a)) [22]. It should be noted that the DPF has very high filtration efficiency when a thin soot layer is formed [24]. Both the flow and the backpressure of the filter are affected by the soot layer formation [35,36]. There is the correlation between the pressure drop with the soot layer growing and the filtration efficiency [37]. Therefore, the PM filtration area of sample A is smaller on initial usage, and resultantly, the soot layer is easily formed on the filter wall, so that the high

filtration efficiency is achieved more rapidly.

To confirm the above explanation, we observed the surface of the filter wall cut from the DPF at the time of two minutes filtration after initial usage. Figure 13 shows a schematic of the cell structure of sample A with SEM image. Here, the inlet side of “a” is the wall surface of the flow toward the outlet channel. The inlet side of “b” is the wall surface of the flow toward the inlet channel. On the other hand, the outlet side of “c” is the wall surface of the flow from the inlet channel. Figure 14 show the SEM images of these wall surfaces at the side of “a”, “b”, and “c”, respectively. At the inlet side of “a”, the gaps of SiC grains are covered by the soot layer. On the other hand, at the inlet side of “b”, there are many gaps of SiC grains. At the outlet side of “c”, the soot layer is not observed, because PM is mainly trapped at the inlet side of the wall surface. From these results, it is confirmed that the soot layer is formed only at the inlet side of the wall surface of the flow toward the outlet channel. That is, the area where the soot layer can be formed is limited, which could be related with the high filtration efficiency of sample A at the earlier stage of the filter usage in Fig. 5.

Next, we examined the initial backpressure based on the inlet and the outlet

aperture ratio. In the case of sample B, the inlet and outlet aperture ratio is equal. On the other hand, in the case of sample A, there are less outlet cells, and the outlet aperture ratio is smaller than that of sample B. Then, in the case of sample A, the flow gathers at the outlet of channel to increase the filter back pressure, which is observed in Fig. 7.

Terregrosa et al. [17] and Piscaglia et al. [30] have investigated the DPF backpressure with soot loading in the numerical simulation to evaluate the pressure drop across the filter and the soot cake formation. Konstandopoulos [38] has presented the following formula for total pressure drop;

$$\Delta P = \Delta P_{expansion} + \Delta P_{outlet\,channel} + \Delta P_{wall} + \Delta P_{inlet\,channel} + \Delta P_{contraction} \quad (3)$$

where total pressure drop ΔP is the sum of the pressure loss of the gas outflow from DPF (ΔP expansion), the pressure loss due to the flow resistance on the outlet channel (ΔP outlet channel), the pressure loss due to filter wall (ΔP wall), the pressure loss due to the flow resistance on the inlet channel (ΔP inlet channel), and the pressure loss of the gas inflow into DPF (ΔP contraction). Because of the accumulated soot in DPF, the

pressure loss due to filter wall (ΔP wall) is largely increased due to the formation of the soot cake.

In the case of sample B, there are four inlet sides of the wall surface, where the soot layer is formed. In the case of sample A, as mentioned previously, there are only three inlet sides of the wall surface on the initial usage. However, as the soot accumulated on the wall from the inlet cell to the outlet cell, making it difficult for the gas to flow, passing through the wall between the inlet cell and the inlet cell would make resistance smaller than passing through the soot layer. In this case, as seen in Fig. 12, the flow passing through the filter substrate wall could occur (flow 2). This tendency has been confirmed in the case of an octagon-square cell DPF [22]. Since there are more inlet areas, the thickness of the soot layer can be thinner. Therefore, the filter capacity of the soot accumulation is high in the case of sample A due to the larger inlet aperture ratio than in the case of sample B. As a result, the backpressure of sample A is lower than that of sample B at the same amount of soot loading.

Finally, we discussed the filter regeneration. Needless to say, the supply of the oxygen is needed for the soot oxidation. Then, it is important to consider the contact

area between the exhaust gas and the soot accumulation is important. As mentioned previously, in the case of sample A, the soot layer could be thin, which reduces the backpressure during soot loading. Therefore, it is considered that the regeneration rate of sample A is higher than that of sample B at the same regeneration temperature, because sample A has larger contact area with exhaust gas, and resultantly, the soot can be reacted with oxygen more efficiently.

5. Conclusions

We compared characteristics between the hexagonal cell DPF and the conventional square cell DPF, especially the PM filtration efficiency and pressure drop and regeneration rate, in order to investigate of the effects of cell geometry on the DPF performances. The following results were obtained.

1. In the case of the hexagonal cell DPF, the particle number concentration decreases more rapidly, and the filtration efficiency is higher. From SEM observation of filter wall, the soot layer is formed only at the inlet side of the wall surface. Then, the area

where the soot layer is formed is limited, and the hexagonal cell DPF has the higher filtration efficiency at the earlier stage of the filter usage.

2. For both samples, the amount of the loaded soot is almost equal at the same soot loading time. The initial backpressure of the hexagonal cell DPF is higher than that of the conventional square cell DPF. However, the backpressure during soot loading of the hexagonal cell DPF is lower when the amount of loaded soot is over 2g/L.

3. Independent of the inlet temperature, the regeneration rate of the hexagonal cell DPF is higher. This is because the contact area between the soot and the exhaust gas is larger.

For further studies, it is necessary to examine the region of thick soot cake, and to make clear the difference between hexagonal and square cell DPFs. In addition, catalyzed hexagonal cell DPF for various conditions will be considered in future.

References

[1] Zervas E, Poulopoulos S, Philippopoulos C, CO_2 emissions change from the introduction of diesel passenger cars: Case of Greece. Energy 2006;31(14):2915-25.
[2] Kennedy IM, The health effects of combustion-generated aerosols. Proceedings of the Combustion Institute 2007;31:2757-70.
[3] Tzamkiozis T, Ntziachristos L, Samaras Z, Diesel passenger car PM emissions: From Euro1 to Euro 4 with particle filter. Atmospheric Environment

2010;44:909-16.
[4] Knecht W, Diesel engine development in view of reduced emission standards. Energy 2008;33(2):264-71.
[5] Torregrosa AJ, Broatch A, Novella R, Mónico LF, Suitability analysis of advanced diesel combustion concepts for emissions and noise control. Energy 2011;36(2) 825-38.
[6] Maiboom A, Tauzia X, Hétet JF, Experimental study of various effects of exhaust gas recirculation (EGR) on combustion and emissions of an automotive direct injection diesel engine. Energy 2008;33(1):22-34.
[7] Bermúdez V, Lujan JM, Pla B, Linares WG, Effects of low pressure exhaust gas recirculation on regulated and unregulated gaseous emissions during NEDC in a light-duty diesel engine. Energy 2011;36(9):5655-65.
[8] Sarvi A, Zevenhoven R, Large-scale diesel engine emission control parameters. Energy 2010;35(2):1139-45.
[9] Neer A, Koylu UO, Effect of operating conditions on the size, morphology, and concentration of submicrometer particulates emitted from a diesel engine. Combustion and Flame 2006;146(1-2):142-54.
[10] Rakopoulos DC, Rakopoulos CD, Giakoumis EG, Dimaratos AM, Characteristics of performance and emissions in high-speed direct injection diesel engine fueled with diethyl ether/diesel fuel blends. Energy 2012;43(1):214-24.
[11] Rakopoulos CD, Dimaratos AM, Giakoumis EG, Rakopoulos DC, Investigating the emissions during acceleration of a turbocharged diesel engine operating with bio-diesel or n-butanol diesel fuel blends. Energy 2010;35(12):5173-84.
[12] Zhu M, Ma Y, Zhang D, An experimental study of the effect of a homogeneous combustion catalyst on fuel consumption and smoke emission in a diesel engine. Energy 2011;36(10): 6004‑9.
[13] Lee WJ, Liu YC, Mwangi FK, Chen WH, Lin SL, Fukushima Y, Liao CN, Wang LC, Assessment of energy performance and air pollutant emissions in a diesel engine generator fueled with water-containing ethanol–biodiesel–diesel blend of fuels.Energy 2011;36(9):5591-9.
[14] Tauzia X, Maiboom A, Shah SR, Experimental study of inlet manifold water injection on combustion and emissions of an automotive direct injection Diesel engine. Energy 2010;35(9):3628-39.
[15] Park J, Yoon J, Song S, Chun KM, Analysis of fractal particles from diesel exhaust using a scanning-mobility particle sizer and laser-induced incandescence. Journal of Aerosol Science 2010;41:531-40.
[16] Tente H, Gomes P, Ferreira F, Amorim JH, Cascao P, Miranda AI, Nogueira L, Sousa S, Evaluating the efficiency of diesel particulate filter in high-duty vehicles: Field operational testing in Portugal. Atmospheric Environment 2011;45:2623-9.
[17] Torregrosa AJ, Serrano JR, Arnau FJ, Piqueras P, A fluid dynamic model for unsteady compressive flow in wall-flow diesel particulate filters. Energy 2011;36:671-84.
[18] Payri F, Broatch A, Serrano JR, Piqueras P, Experimental-theoretical methodology for determination of inertial pressure drop distribution and pore structure properties in wall-flow diesel particulate filters (DPFs). Energy 2011;36:6731-44.
[19] Dilip K, Vasa NJ, Carsten K, Ravindra KU, Incineration of diesel particulate matter using induction heating technique. Applied Energy 2011;88:938‑46.
[20] Liati A, Eggenschwiler DP, Gubler EM, Schreiber D, Aguirre M, Investigation of

diesel ash particulate matter: A scanning electron microscope and transmission electron microscope study. Atmospheric Environment 2012;49:391-402.
[21] Liati A, Eggenschwiler DP, Characterization of particulate matter deposited in diesel particulate filters: Visual and analytical approach in macro-, and micro- and nano-scales. Combustion and Flame 2010;157:1658-70.
[22] Ogyu K, Ohno K, Hong S, and Komori T, Ash storage capacity enhancement of diesel particulate filter. In: SAE Technical Paper 2004-01-0949; 2004.
[23] Ogyu K, Oya T, Ohno K, and Konstandopolous GA, Improving of the filtration and regeneration performance by the SiC-DPF with the layer coating of PM oxidation catalyst. In: SAE Technical Paper 2008-01-0621; 2008.
[24] Tsuneyoshi K, Takagi O, Yamamoto K, Effects of washcoat on initial PM filtration efficiency and pressure drop in SiC DPF. In: SAE Technical Paper 2011-01-0817; 2011.
[25] Amirnordin SH, Seri SM, Salim WSW, Rahman HA, Hasnan K, Pressure drop analysis of square and hexagonal cells and its effects on the performance of catalytic converters. International Journal of Environmental Science and Development 2011;2(3):239-47.
[26] Lapuerta M, Oliva F, Agudelo JR, Boehman AL, Effect of fuel on the soot nanostructure and consequences on loading and regeneration of diesel particulate filters. Combustion and Flame 2012;159:844-53.
[27] Jacob JS, David BK, Winthrop FW, David DG, Martyn VT, Influence of storage and release on particle emissions from new and used CRTs. Atmospheric Environment 2009;43:3998-4004.
[28] Bergmann M, Kirchner U, Vogt R, Benter T, On-road and laboratory investigation of low-level PM emissions of a modern diesel particulate filter equipped diesel passenger car. Atmospheric Environment 2009;43:1908-16.
[29] Kulkarni P, Baron PA, Willeke K, Aerosol measurement: principles, techniques and applications. Wiley 2011;3rd Edition. Reference to a book: ISBN 2011, 978-0-470-38741-2.
[30] Piscaglia F, Ferrari G, A novel 1D approach for the simulation of unsteady reacting flows in diesel exhaust after-treatment systems. Energy 2009;34:2051-62.
[31] Song J, Wang J, Boehman AL, Examination of the oxidation behavior of biodiesel soot. Combusttion and Flame 2006;146:73-84.
[32] Lee SJ, Jeong SJ, Kim WS, Numerical design of the diesel particulate filter for optimum thermal performances during regeneration. Applied Energy 2009;86:1124‑35.
[33] Yamamoto K, Nakamura M, Takada N, Misawa M, Combustion simulation with Lattice Boltzmann method in a three-dimentional porous structure. Proceedings of the Combustion Institute 2005;30:1509-15.
[34] Yamamoto K, Yamauchi K, Takada N, Misawa M, Furutani H, Shinozaki O, Lattice Boltzmann simulation on continuously regenerating diesel filter. Philosophical Transactions A Mathematical Physical & Engineering Science 2011;369:2584-91.
[35] Yamamoto K, Satake S, Yamashita H, Microstructure and particle-ladan flow in diesel particulate filter. International Journal of Thermal Sciences 2009;48:303-7.
[36] Yamamoto K, Oohori S, Yamashita H, Daido S, Simulation on soot deposition and combustion in diesel particulate filter. Proceedings of the Combustion Institute 2009;32:1965-72.
[37] Bensaid S, Marchisio DL, Russo N, Fino D, Experimental investigation of soot

deposition in diesel particulate filters. Catalysis Today 2009;147S:S295-S300.
[38] Konstandpoulos AG, Flow resistance descriptors for diesel particulate filters: definitions, measurements and testing. In: SAE Technical Paper 2003-01-0846; 2003.

LIST OF FIGURES

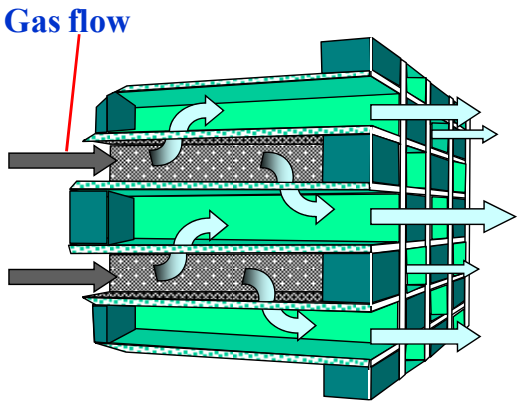

Fig. 1. Image of a wall-flow DPF.

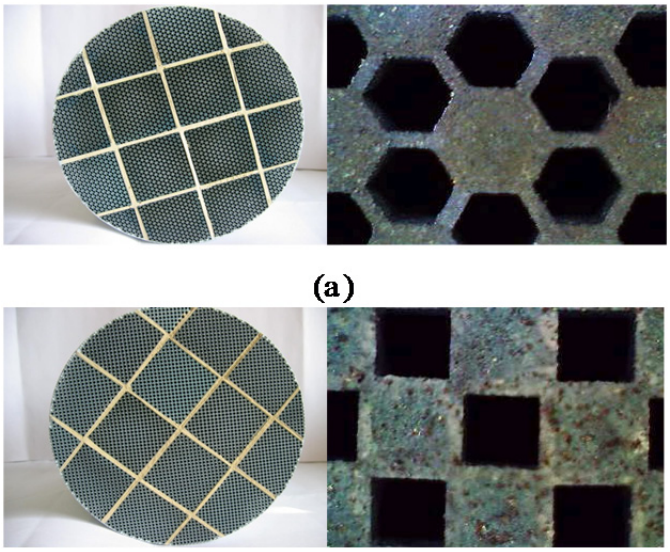

Fig. 2. Appearance and cell designs of (a) a hexagonal cell DPF, (b) a square cell DPF.

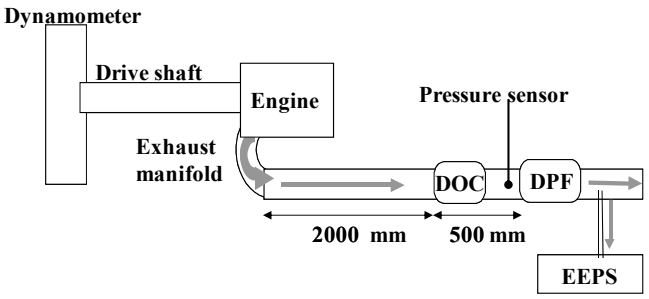

Fig. 3. Experimental setup.

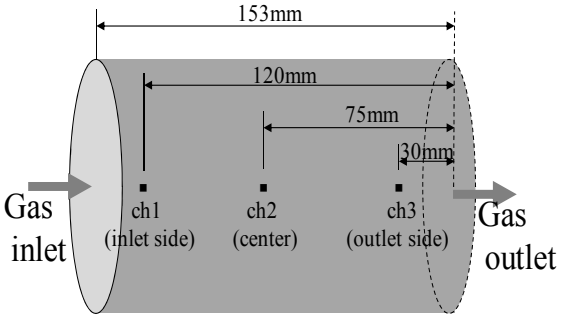

Fig. 4. Positions of thermocouples during the regeneration test.

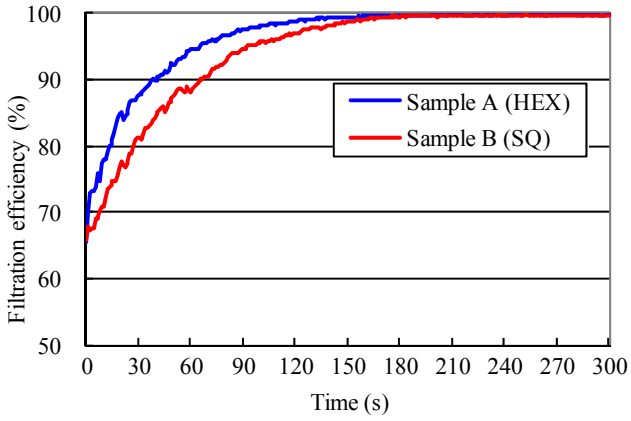

Fig. 5. Number-based filtration efficiency upon initial usage for each sample.

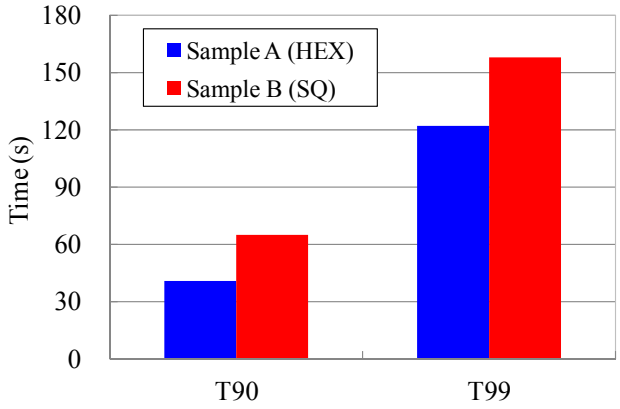

Fig. 6. Comparison for T90 and T99 for each sample.

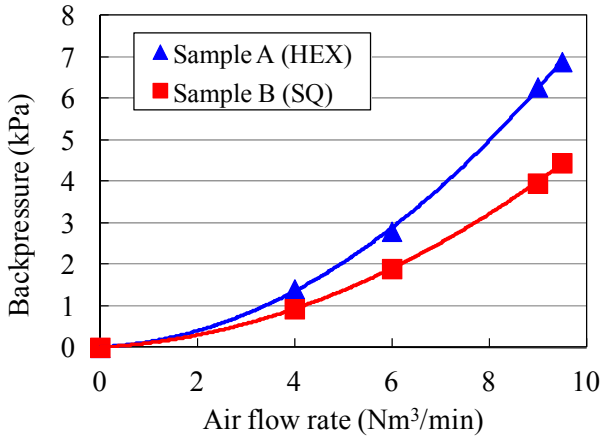

Fig. 7. Relationship between initial backpressure and air flow rate (no PM loading).

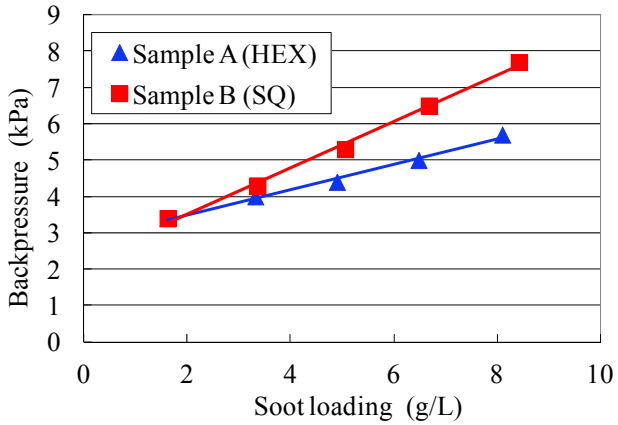

Fig. 8. Backpressure during soot loading for each sample.

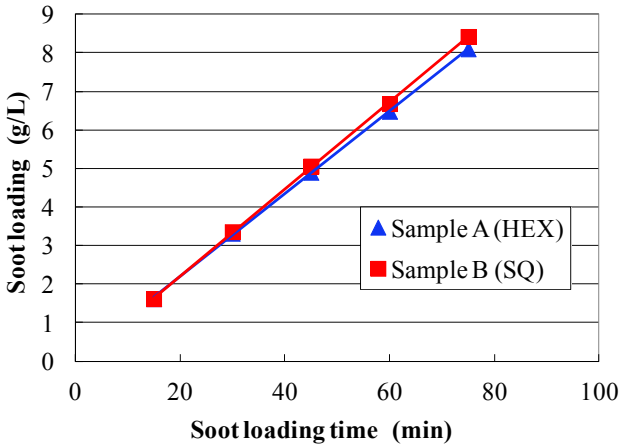

Fig. 9. Relationship between soot loading time and the amount of soot loading for each sample.

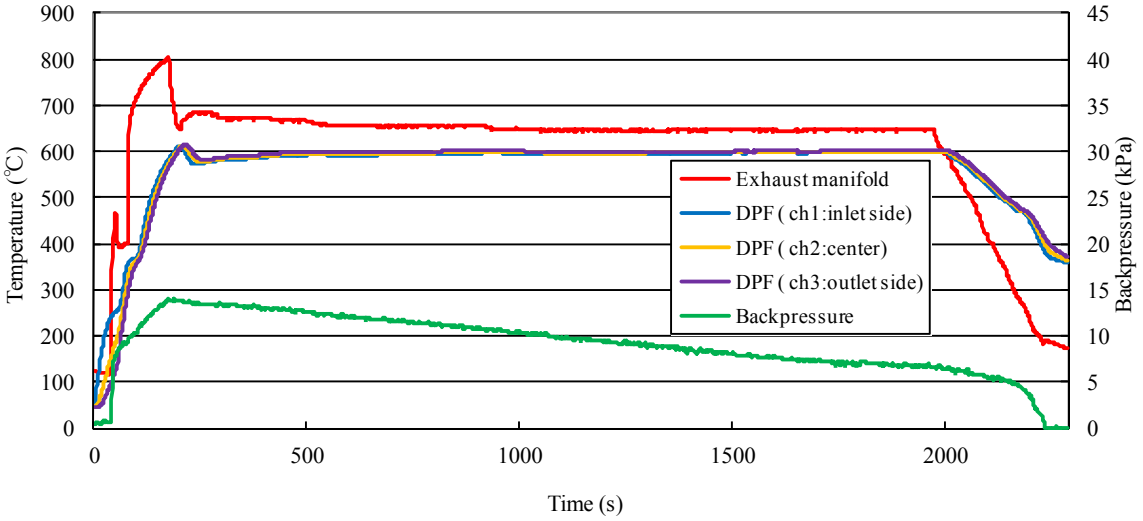

(a)

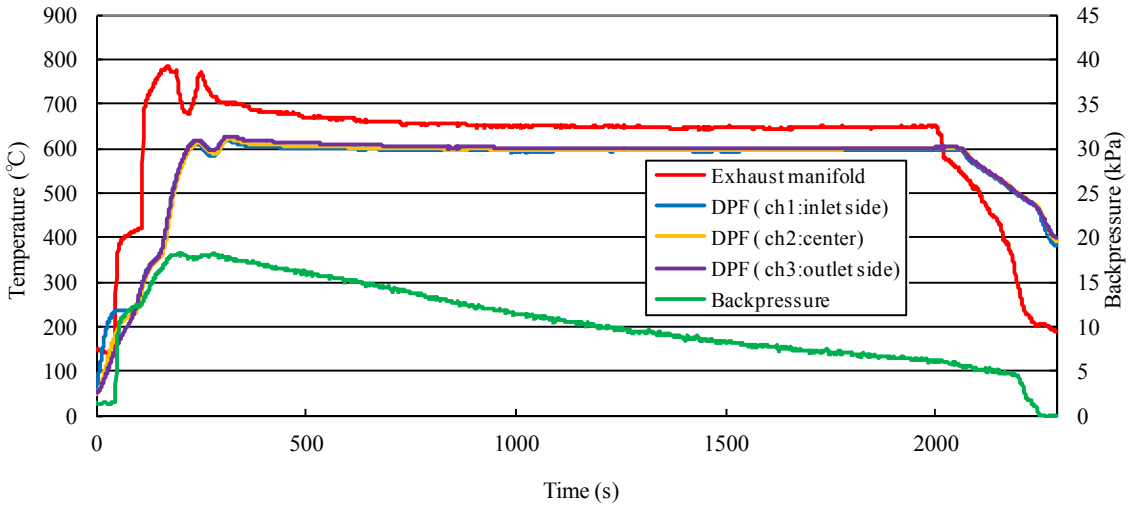

(b)

Fig. 10. Time-variation of each temperature and backpressure during the regeneration test of (a) sample A and (b) sample B (test condition 3).

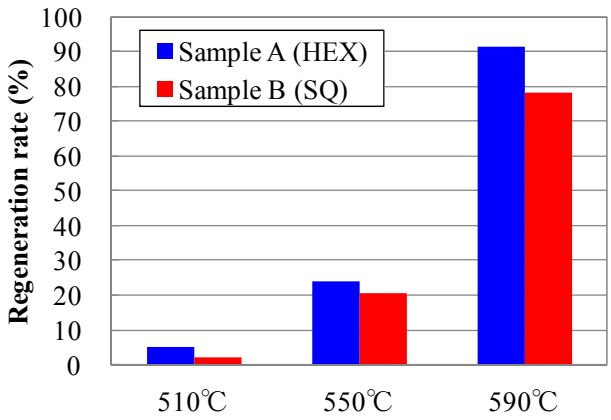

Fig. 11. Regeneration rate at different inlet temperature.

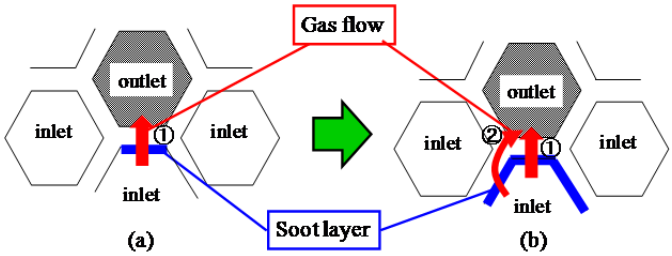

Fig. 12. Flow of exhaust gas in hexagonal cell DPF; (a) small soot amount at initial usage, (b) large soot amount with thick soot cake formation. Flow 1 is directly from inlet cell to outlet cell, and flow 2 is from inlet cell to outlet cell through the filter substrate wall.

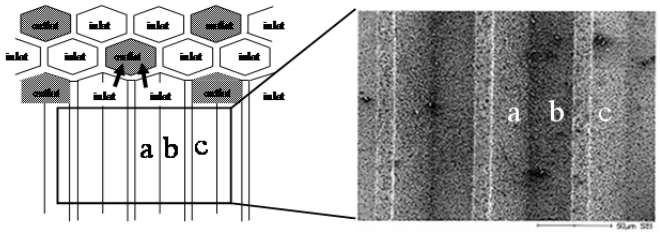

Fig. 13. A schematic of cell structure of sample A with SEM image. Inlet side "a" is wall surface of the flow toward outlet channel. Inlet side of "b" is wall surface of the flow toward inlet channel. Outlet side of "c" is wall surface of the flow from inlet channel.

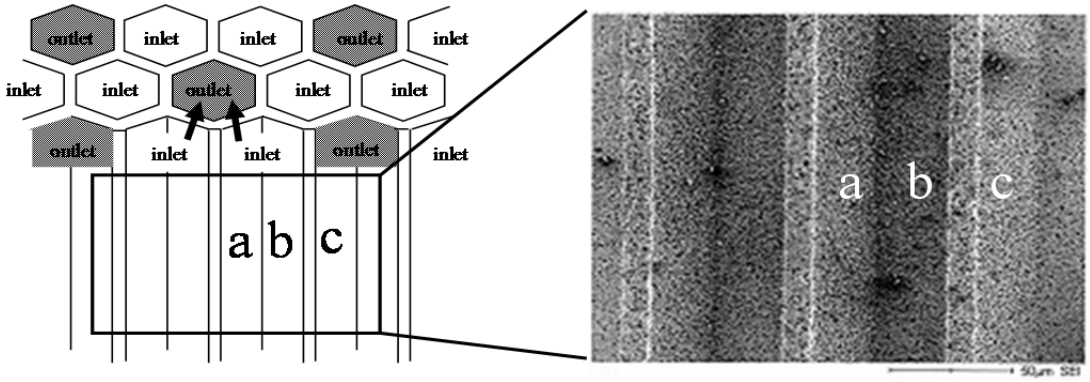

Fig. 13. (enlarged)

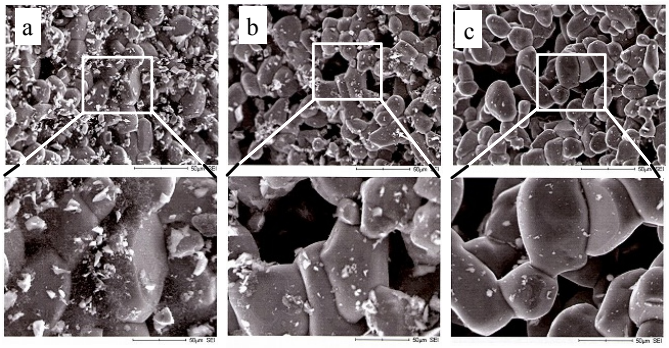

Fig. 14. SEM images of wall surfaces at the side of “a”, “b”, and “c” in Fig. 13.

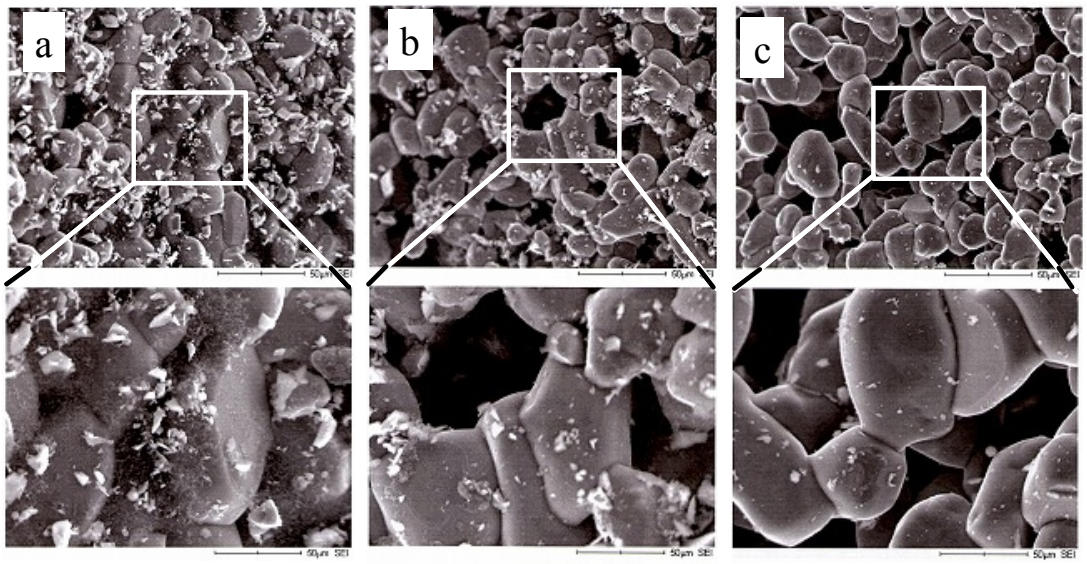

Fig. 14. (enlarged)

Table 1 DPF specifications

Sample	A	B
Substrate	SiC (silicon-carbide)	
Size (mm)	D144, L153	
Cell Geometry	Hexagon	Square
Cell Density (cpsi)	300	300
Wall Thickness (mm)	0.25	0.25
Open Frontal Area (%)	46.2	34.2
Open Rear Area (%)	22.6	34.2
Porosity (%)	46.3	46.5
Average Pore Diameter (μm)	16.0	16.8
Washcoat	none	none
Pt Loading	none	none

Table 2 Engine specifications

Model	NISSAN QD32
Engine Type	4 stroke, swirl chamber type diesel
Cylinders	inline-4
Valve Mechanism	OHV
Displacement	3.153 L
Rated Power	72 kW @ 3600 rpm
Peak Torque	216 Nm @ 2000 rpm
EGR System	none
Turbocharger	none (NA)

Table 3 Conditions in DPF regeneration test

Test condition	1	2	3
Revolution per minute	3000	3000	3000
Throttle angle (%)	65	68	70
Torque (Nm)	100 ±5	110 ±5	120 ±5
Exhaust gas temp (°C)	550 ±10	600 ±10	650 ±10
DPF temp (°C)	510 ±10	550 ±10	590 ±10
O_2 concentration (%)	9.4	8.2	7.2
Keeping time (min)	30	30	30

Table 4 Comparison of test results

Sample	A (HEX)	B (SQ)
Filtration efficiency	O	
Initial pressure loss		O
Pressure loss during soot loading	O	
Regeneration rate	O	